The Astrophysical Journal, 796:33 (15pp), 2014 November 20 doi:10.1088/0004-637X/796/1/33

THE FORMATION AND LAUNCH OF A CORONAL MASS EJECTION FLUX ROPE: A NARRATIVE BASED ON OBSERVATIONS

T. A. Howard and C. E. DeForest
Southwest Research Institute, 1050 Walnut Street, Suite 300, Boulder, CO 80302, USA; howard@boulder.swri.edu
Received 2014 May 27; accepted 2014 September 17; published 2014 November 3

ABSTRACT

We present a data-driven narrative of the launch and early evolution of the magnetic structure that gave rise to the coronal mass ejection (CME) on 2008 December 12. The structure formed on December 7 and launched early on December 12. We interpret this structure as a flux rope based on prelaunch morphology, postlaunch magnetic measurements, and the lack of large-scale magnetic reconnection signatures at launch. We ascribe three separate onset mechanisms to the complete disconnection of the flux rope from the Sun. It took 19 hr for the flux rope to be fully removed from the Sun, by which time the segment that first disconnected was around 40 $R_\odot$ away. This implies that the original flux rope was stretched or broken; we provide evidence for a possible bisection. A transient dark arcade was observed on the Sun that was later obscured by a bright arcade, which we interpret as the strapping field stretching and magnetically reconnecting as it disconnected from the coronal field. We identify three separate structures in coronagraph images to be manifestations of the same original flux rope, and we describe the implications for CME interpretation. We cite the rotation in the central flux rope vector of the magnetic clouds observed in situ by *ACE*/*Wind* and *STEREO-B* as evidence of the kink instability of the eastern segment of the flux rope. Finally, we discuss possible alternative narratives, including multiple prelaunch magnetic structures and the nonflux rope scenario. Our results support the view that, in at least some CMEs, flux rope formation occurs before launch.

Key words: solar wind – Sun: corona – Sun: coronal mass ejections (CMEs) – Sun: filaments, prominences – Sun: magnetic fields

Online-only material: animations, color figures

1. INTRODUCTION

Magnetic flux ropes are known to often lie within coronal mass ejections (CMEs). Many CME initiation models require the presence of a flux rope (e.g., Hood & Priest 1981; Martin et al. 1985; van Ballegooijen & Martens 1989; Chen 1989; Titov & Démoulin 1999; Török & Kleim 2003, 2005; Fan & Gibson 2003, 2004), whereas others describe the formation of a flux rope as a consequence of the CME launch (e.g., Sturrock 1989; Antiochos et al. 1999; Lynch et al. 2008; Panasenco et al. 2011). These models describe a highly structured magnetic field in an approximately cylindrical shape that is either disconnected from and suspended within the surrounding coronal field prior to launch, or is removed from the coronal field during launch via magnetic reconnection. Understanding which of these processes is responsible for the launch of CME flux ropes is critical to understanding the physics of CME formation and evolution.

CME flux ropes have been detected in situ by spacecraft for over 30 years as periods of smooth rotation in the magnetic field, such as in the passage of magnetic clouds (MCs; Burlaga et al. 1981). MCs have three signatures in situ: high magnetic field strength, low temperature, and a rotating field structure (Burlaga et al. 1981; Klein & Burlaga 1982). They are also often associated with low density (e.g., Lepping et al. 1990; Lynch et al. 2003), but this is not a required or reliable signature for an in situ MC (Lepping & Berdichevsky 2000). The increased strength and the high level of structure of the field comprising the clouds have led to the conclusion that they are magnetic flux ropes (e.g., Goldstein 1983; Marubashi 1986; Lepping et al. 1990; Bothmer & Schwenn 1998), and the low density (when observed) has been attributed to an evacuation of material that is due to pressure balance effects from the increased magnetic pressure, decreased thermal pressure, and subsequent expansion within the cloud (e.g., Low 1993; Bothmer & Schwenn 1998; Davis et al. 2009).

When observed in situ near 1 AU, MCs are detected in 30%–50% of CMEs (Gosling 1990; Cane et al. 1997), and a solar cycle dependence of MC presence within in situ CMEs has been reported (Cane & Richardson 2003). It is not clear from existing studies whether this is a solar cycle effect on the nature of individual CMEs or on the likelihood that a given flux rope will impact a spacecraft at low ecliptic latitude. The proportion of CMEs that contain flux ropes is a topic with a high level of interest in the solar physics community at present (e.g., Vourlidas et al. 2013, and the associated Solar Physics volume dedicated to this topic).

Connections of in situ measurements with coronagraph observations of CMEs are made using heliospheric imagers, which image the solar wind in visible white light (Eyles et al. 2003, 2009). With properly processed heliospheric imager data, such as those developed by DeForest et al. (2011), we can identify the cavity component of a CME in the heliospheric imager data and trace it to the reduction in density often associated with MCs. Likewise, the CME void can be traced back in time through the heliospheric imager data set to its coronagraph origins. This was accomplished by Howard & DeForest (2012), who observationally confirmed the commonly held belief (e.g., Forbes et al. 2006) that the cavity component of the "classic" three-part CME (Illing & Hundhausen 1985) was, in one case at least, the component that became the in situ MC.

When they are close to the Sun (i.e., in the low corona), CME flux ropes are difficult to observe because measurements of the coronal magnetic field remain limited despite spectacular recent advances with CoMP (Tian et al. 2013, and references

therein), and their often-reduced density renders them poorly visible to the current generation of solar imagers. We search for circularly shaped voids in solar EUV imager data and connect them with the cavity component of a three-part CME after they are launched (e.g., Howard & DeForest 2012; DeForest et al. 2013). Efforts to accomplish this have been made by many workers (e.g., Illing & Hundhausen 1985; Wood et al. 1999; Gibson 2005; Patsourakos et al. 2010; Temmer et al. 2010). Although it is generally accepted that in such cases the erupting magnetic structure is a flux rope, it remains an open question whether the flux rope is present prior to launch (e.g., Panasenco et al. 2013).

In this paper, we present a narrative of the formation and launch of a single CME flux rope using observations from imaging and in situ data sets. The flux rope, part of which caused the CME of 2008 December 12, launched asymmetrically, with the trailing segment departing the Sun 18 hr after the leading segment, by which time the complete flux rope spanned a radial distance of some 40 $R_\odot$. The prelaunch magnetic structure formed days prior to launch. We have previously reported on the association between this CME's cavity and its manifestation in the heliosphere (Howard & DeForest 2012) and used that association to connect the coronal structure prior to and at launch with features observed in situ as the CME passed Earth (DeForest et al. 2013). In the present report, which presents additional scientific revelations not yet discussed regarding greater CME flux rope dynamics, we focus on the launch of the entire flux rope, end to end, and provide our best attempt at a narrative of the physical processes describing its complete launch. We find the launch process to be highly complex for what was observed as a simple, slow CME, requiring no less than 18 hr, three onset mechanisms, and a possible bisection to completely remove it from the corona. This led to some surprising observational results in the white-light images, which we present with a note of caution to those analyzing coronagraph and heliospheric imager observations of CMEs. We also provide an explanation for the reversal in the rotation of the MC field vector observed at *ACE*/*Wind* and *STEREO-B*. Finally, we explore two possible alternative narratives: that of multiple prelaunch magnetic structures and a nonflux rope prelaunch scenario.

2. DATA AND THE "EVENT"

We used the same data sets that we used for other studies of this "event". The reader is referred to DeForest et al. (2011, 2013), Howard & DeForest (2012), and Howard et al. (2012) for more details. Briefly, we use observations from the Extreme Ultra-Violet Imager (EUVI) on board the *Solar-Terrestrial Relations Observatory* (*STEREO*). The EUVI forms part of the Sun Earth Connection Coronal and Heliospheric Investigation (SECCHI) imager suite on board *STEREO* (Howard et al. 2008a), and apart from our discussion of the COR2 coronagraph and HI-1 heliospheric imager observations in Section 4, we focus on EUVI. New for this paper, we have added observations from the Extreme-Ultraviolet Telescope (EIT) on board the *Solar and Heliospheric Observatory* (*SOHO*; Delaboudinière et al. 1995).

The CME and the part of the flux rope associated with it began its launch from the Sun in the early hours (UT) on 2008 December 12. An exhaustive investigation of this CME as observed with white-light imagers and in situ instruments has been made by the authors in a series of four papers cited in the previous paragraph, and we draw the reader's attention to additional studies on this CME reported by other workers (Davis et al. 2009; Liu et al. 2010; Lugaz 2010; Byrne et al. 2010; Panasenco et al. 2011, 2013). We do not revisit these results here, except to state that the CME was slow (~400 km s^{-1}), was not associated with a bright solar flare, did not drive an interplanetary shock in the solar wind, and while it did impact the Earth was only marginally geoeffective. Most importantly, however, this CME occurred at a time when the *STEREO* spacecraft were at quadrature (i.e., at 45° angular separation from the Sun–Earth vector and at 90° from each other). This afforded a unique opportunity to observe the CME and its flux rope from almost exactly perpendicular lines of sight. The importance of perspective cannot be overstated when analyzing CMEs observed with white-light imagers (e.g., Webb et al. 1998; Burkepile et al. 2004; Howard et al. 2008b, 2012), and we found for this event (DeForest et al. 2013, and the results in the present paper) that it is important when using EUV imagers as well.

2.1. Recap of Previous Observations of the 2008 December 12 Flux Rope

The most recent paper in our series on the 2008 December 12 CME (DeForest et al. 2013, their Section 3.4) described the launch of the leading end of its flux rope by connecting features observed by EUV cameras across the solar disk with features observed by coronagraphs. We identified the part of the flux rope that formed the CME and the part that eventually impacted the in situ spacecraft near 1 AU and the Earth. Figure 1 shows the two EUVI (from *STEREO-A* and *STEREO-B*) and EIT images with a diagram of the appearance of the likely magnetic structure prior to the initial onset. The configuration of this prelaunch structure was constructed with the assistance of the potential field source surface (PFSS) model (see Section 5.1 for more details).

We described the launch of the flux rope in sections, starting with its western part disconnecting from 03:30 to 06 UT via the tether cutting mechanism (Sturrock 1989; Moore & Sterling 2006). This initial disconnection was manifested as a small flare in an active region at one end of the pre-event structure. Because the overlying cavity, which we interpret as a preformed flux rope, does not begin to move until after the initial flare around 03 UT, we interpret the initial flare as the causal signature of the initial launch of the flux rope, and there is no indication of any related structure launching before this flare. As this end of the structure, henceforth called the western segment and indicated by the green loops in Figure 1, rose, a filament was observed (with EUVI-B) to roll over the top of the structure and pour into the Sun at around 06:10 UT. The entry of the filament material is visible as a flaring region on the solar disk to the southwest of the original flare site, visible by both EUVI-A and EIT. DeForest et al. (2013) describe this as a mass-draining (e.g., Klimchuk & Sturrock 1992; Fong et al. 2002; Zhang & Low 2004) mechanism that enables the launch of the middle part, henceforth called the central segment (the magenta loops) of the flux rope. It is this central segment that drives the CME identified as the December 12 "partial halo," first observed by LASCO C2 on board *SOHO* at 08:54 UT, that impacted the Earth. The other end of the flux rope, henceforth called the eastern segment (the red loops), identified as a cavity suspended over the solar limb in EUVI-A, is seen to twist around at 16 UT and finally to launch at 22 UT. We attributed its launch to the kink instability mechanism (Török & Kleim 2003, 2005; Fan & Gibson 2003, 2004; Rachmeler et al. 2009).

DeForest et al. (2013) interpreted the prelaunch magnetic structure as a flux rope because of the circular cavity present

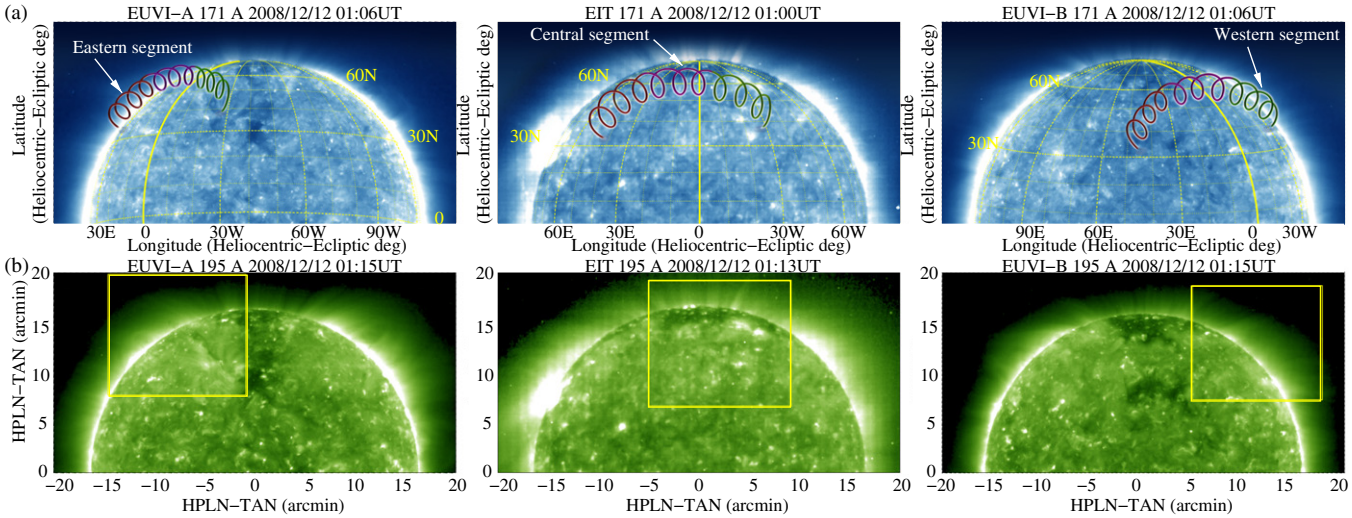

Figure 1. (a) 171 Å images from (left) EUVI-A, (middle) EIT, and (right) EUVI-B around 01 UT on 2008 December 12 with an Earth-ecliptic-centered Stonyhurst grid superimposed. (b) 195 Å images from the same respective instruments as the top row from around the same time. Panel (a) shows an illustration of the prelaunch flux rope spanning the corona. We divide the flux rope into three segments: eastern (red), central (magenta), and western (green). This color configuration corresponds to the overlaid diagrams shown in DeForest et al. (2013, their Figures 6 and 7). The western segment launched first, and 18 hr later the eastern segment finally left the Sun. The magenta component indicates the central segment that impacted the Earth. For the purpose of image cadence optimization, our subsequent figures present only images from the 171 Å band (blue) from EUVI and 195 Å from EIT (green). Later figures are zoomed-in versions of these panels, with the areas shown by the yellow boxes in Panel (b).

(A color version of this figure is available in the online journal.)

throughout the five days leading up to its launch and the behavior of the surrounding structure during its launch. We now expand this narrative to a fuller description of the launch of the entire flux rope structure and discuss important physical implications for flux rope and CME observation and measurement. Among the evidence we provide for the existence of a prelaunch flux rope, we describe in this paper the cross-sectional scan of the entire structure and of the swirling motion of related material in the days leading up to the launch. These are in Section 3.2.

Our latest detailed study into this unique combination of observations yielded important new scientific revelations about the greater structure surrounding this CME, and about CMEs in general, that to our knowledge have not been discussed in prior literature. In particular, we explore the prelaunch configuration via what we term a cross-sectional scan, the asymmetric nature of the flux rope eruption, the multiple-onset mechanisms required for the disconnection of this single flux rope from the Sun, and its possible bisection during launch. We explore the extension of the kink instability launch mechanism to observations at 1 AU and discuss the important implications of observing extended three-dimensional (3D) structures with white-light imagers. These warranted this additional (and final) publication in our series of papers exploring this event during a unique period of the *STEREO* mission.

3. NEW OBSERVATIONS

Figure 2 shows a sequence of stills from the accompanying movie (digital supplement) showing the EUVI-A 171 Å (left), EIT 195 Å (center), and EUVI-B 171 Å (right) views of the lifetime of the flux rope regarding its connection to the Sun. This movie shows the initial formation (Panel (a)), its initial launch (b), the filament drain (c), and the final disconnection (d). In this section we describe observations that are additional to our prior work and offer a consistent physical explanation for their occurrences.

3.1. Expansion En Route to 1 AU

Notice that the central (magenta) segment in Figure 1, which was established by DeForest et al. (2013) as the part of the flux rope that impacted the Earth, is considerably to the north of the radial projection of the Earth onto the solar disk (at 0° latitude). This shows that the central segment of the flux rope arrived some 50° southward en route to 1 AU. We see in the SECCHI movies from Howard & DeForest (2012) and Howard et al. (2012) that there is a strong nonradial southern motion of the December 12 CME in the coronagraphs and in EUVI from the results by DeForest et al. (2013). The works of Panasenco et al. (2011, 2013) describe the strong nonradial eruption of the filament. The 3D reconstruction work of Byrne et al. (2010) showed both a southern deflection of around 30° and an early overexpansion of this CME, followed by constant expansion afterward. Combining the expansion with the deflection is sufficient for this segment to cross the Sun–Earth line by the time it reached 1 AU.

3.2. Formation and Prelaunch Configuration

Figure 3 is a sequence of frames from the accompanying EUVI-A movie (digital supplement) showing the likely initial formation of the magnetic structure, which our primary narrative describes as a prelaunch flux rope. The first signs of formation (Panel (a)) appear around 05 UT on December 7, with a coherent churning motion above what eventually becomes the filament. At around 07:30 UT a loop begins to form in the same region, shown fully formed at 10:01 UT in Panel (b). This loop twists, starting around 11 UT (shown at 13:41 UT in Panel (c)), and by 18 UT a complete circular cavity has formed with a long radial filament channel beneath it. Panel (d) shows this configuration at 19:31 UT, well after the formation and some 4.5 days before the eruption.

Throughout the days following December 7 leading up to the launch on December 12, we continually observe the flux rope suspended over the limb in EUVI-A, as can be seen in the

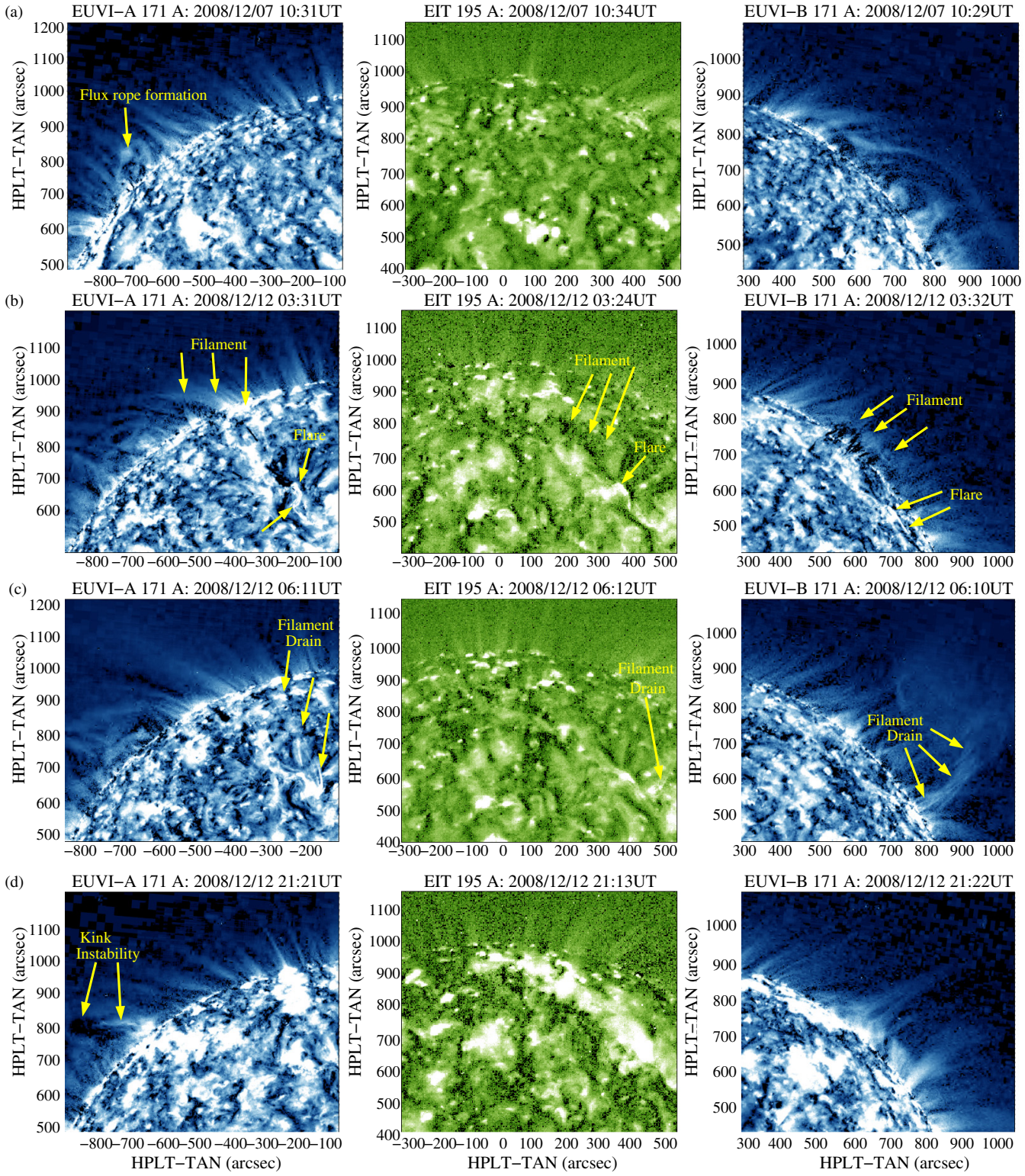

Figure 2. Stills from an accompanying movie showing the lifetime of the CME flux rope. The left column shows frames from EUVI-A (171 Å), the center column is for EIT (195 Å), and the EUVI-B (171 Å) is to the right. The images are zoomed in on the area of interest, indicated by the yellow boxes in the bottom row of Figure 1. We have selected frames of features of interest, starting with (a) the initial formation early on December 7; (b) the flare around 03:30 UT on December 12 that initiates the launch of the western segment of the flux rope; (c) the mass draining that enables the launch of the central segment; and finally (d) the kink instability around 22 UT on December 12 that disconnects its eastern segment. In each panel, features of interest are indicated with arrows and labeled.

(An animation and a color version of this figure are available in the online journal.)

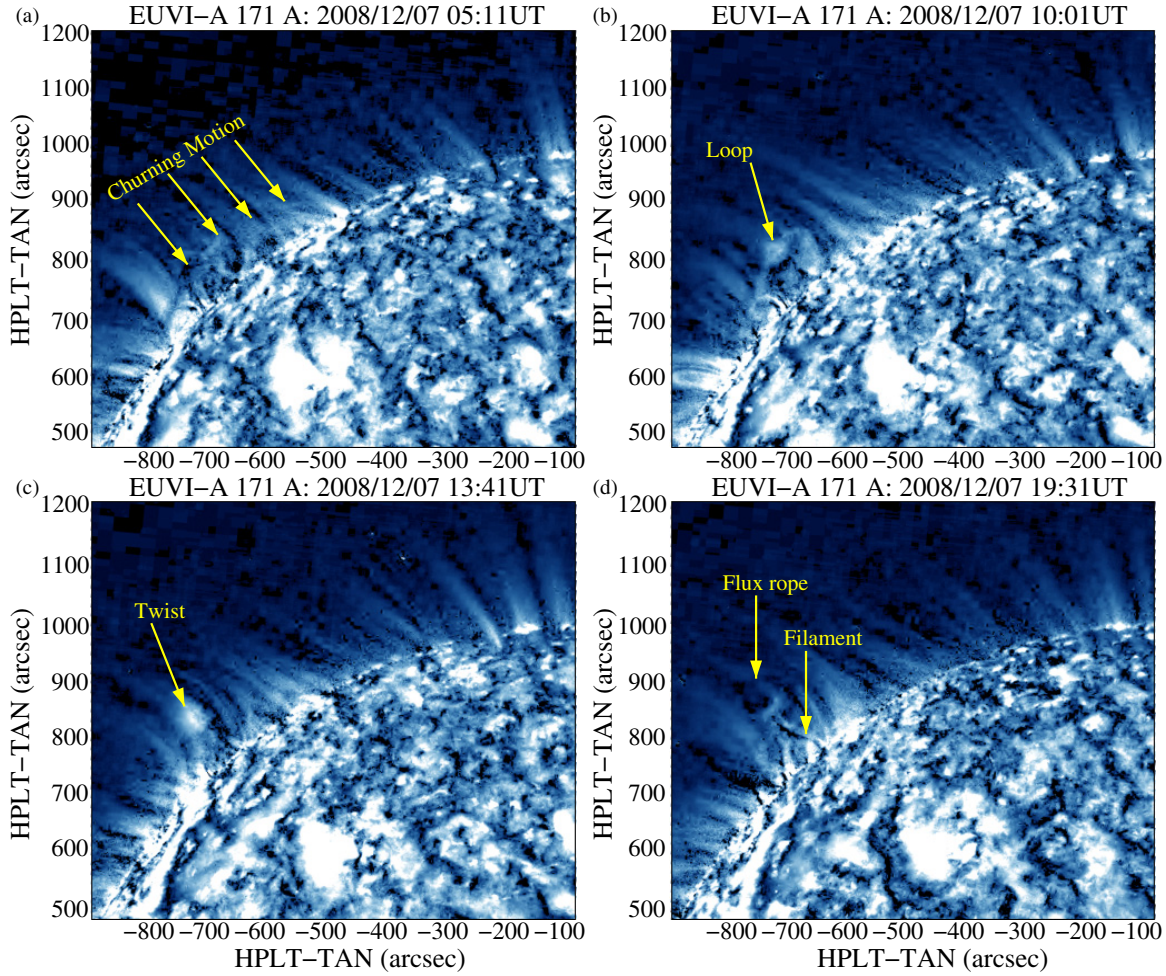

Figure 3. EUVI-A 171Å images from the movie showing the likely initial formation of the flux rope in the morning of 2008 December 7. Images have been selected from (a) 05:11 UT, (b) 10:01 UT, (c) 13:41 UT, and (d) 19:31 UT. The arrows indicate the features discussed in the text.

(An animation and a color version of this figure are available in the online journal.)

accompanying digital movie. Because the Sun rotates over 60° during this time, we are continuously observing the off-limb aspect of the rope, which approximates a cross-sectional scan; as the Sun rotates westward we continually observe new cross sections as they cross the EUVI-A sky plane. We note a few changes that occur during the scan. First, during December 9 there are topological changes that carry away some of the twist; this is manifested by swirling motions that translate feature brightness toward the south. Second, the location of the flux rope relative to the solar "surface" changes throughout the scan. On December 7, immediately after its formation, the cavity is suspended well above the solar disk, with a wide radial filament connecting it to the Sun. By December 12 the cavity appears to be sitting on or very near the solar surface. This would indicate that either the flux rope initially formed above the solar disk and moved downward later, or that the western segment was always above the disk and the eastern segment was always closer to it. There is insufficient information from the movie alone to identify which of these two scenarios is most likely.

3.3. Filament Eruption

The nature of the filament material within the magnetic structure that becomes a CME varies depending on the model describing the prelaunch magnetic configuration. While the vast majority describe their formation along the polarity neutral line, their location relative to the magnetic structure that becomes the CME depends on whether the model regards the flux rope as preformed or not. Because our primary narrative (depicted in Figure 9) involves a preformed flux rope, we describe the prelaunch filament in its simplest terms: as an accumulation of cool material along the base of the flux rope. Figure 4 shows an EUV image sequence from 05:40 to 06:30 UT, with two features indicated: we describe the "anchor field" (Section 5) as a single loop wrapping over the top of the central segment and looping within the western segment. We see this loop moving away from the Sun (labeled with the white arrows) in Panels (a), (b), and (c). Some of the material contained by this loop rolls over the top of the western segment and pours into the Sun, indicated by the yellow arrows in Panels (b) and (c). The departure of a dark filament is also visible in the EIT movie, but it is difficult to observe in the still frames. We interpret this as an indication of the departure of the bottom part of the original flux rope, where it is widely believed that filament material accumulates (e.g., López Ariste et al. 2006, and references therein). Assuming that the filament is suspended at the bottom of the flux rope provides a good indicator of the span across the solar disk of the rope. Note also that the filament departs immediately prior to the appearance of the filament draining (brightening) feature to the southwest of the initial flare site at around 06 UT, and it is coincident with the filament material rolling over the

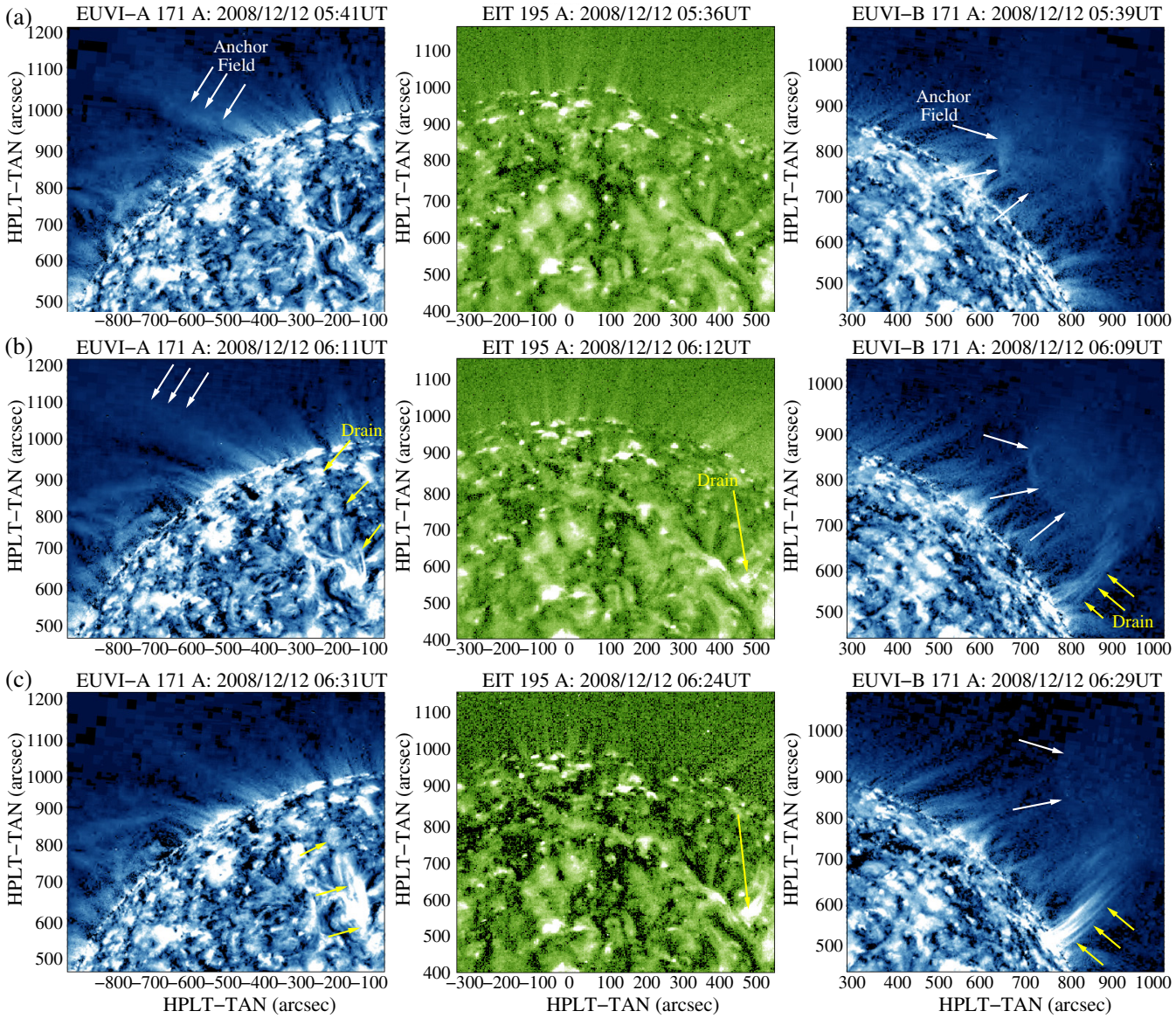

Figure 4. EUVI 171 Å and EIT 195 Å images showing the launch of the central segment of the flux rope. Times are from around (a) 05:40 UT, (b) 06:10 UT, and (c) 06:30 UT. Two features are indicated: an "anchor field" that we interpret as a single loop holding the central segment to the Sun that is seen to depart the Sun, and a "drain" that indicates the removal of filament material from the anchor field. This is an indicator of the departure from the Sun of the central segment of the flux rope, and the draining filament feature is highlighted by DeForest et al. (2013) as evidence of mass draining (and is also shown in Figure 2(c)).

(An animation and a color version of this figure are available in the online journal.)

top of the loop prior to its draining. The temporal coincidence of this sequence of events and the visible acceleration of the anchor field support the suggestion by DeForest et al. (2013) that the draining of the filament material enabled the launch of the central segment.

A simple explanation is that a single magnetic loop was originally oriented such that it passed over the top of the central segment, looped somewhere at the bottom and within the western segment, passed over the top of the remainder of the western segment, and connected with the Sun to the southwest of the original flare site. As with the flux rope, this loop held filament material at its base, which served as an anchor such that its eastern component held the central segment of the flux rope to the Sun (hence our selection of the term "anchor field"). Prior to launch, the central segment is held in place by tension from the overlying strapping field plus the anchor field and additionally from gravitational forces from the mass stored within the anchor field. The system requires only a small disturbance to break the equilibrium, which we attribute to removal of the latter (visible as material draining into the Sun by EUVI-B). This is sufficient to begin the departure of the central segment, which is accelerated when the field lines were dragged beneath the expanding segment and reconnect.

3.4. Evidence of Field Stretching and Magnetic Reconnection

Figure 5 shows a sequence of EUVI-A, EIT, and EUVI-B images from 06:10 to 08 UT with the passage of a front across the corona indicated. This front is directly below the central segment: the part that left the Sun at 04:40 UT and eventually impacted the Earth. A dark front is first visible moving northward, with a bright front following immediately behind. By 08 UT the dark front has been engulfed by the following bright front. Its timing and location relative to those of the erupting western segment is strongly indicative

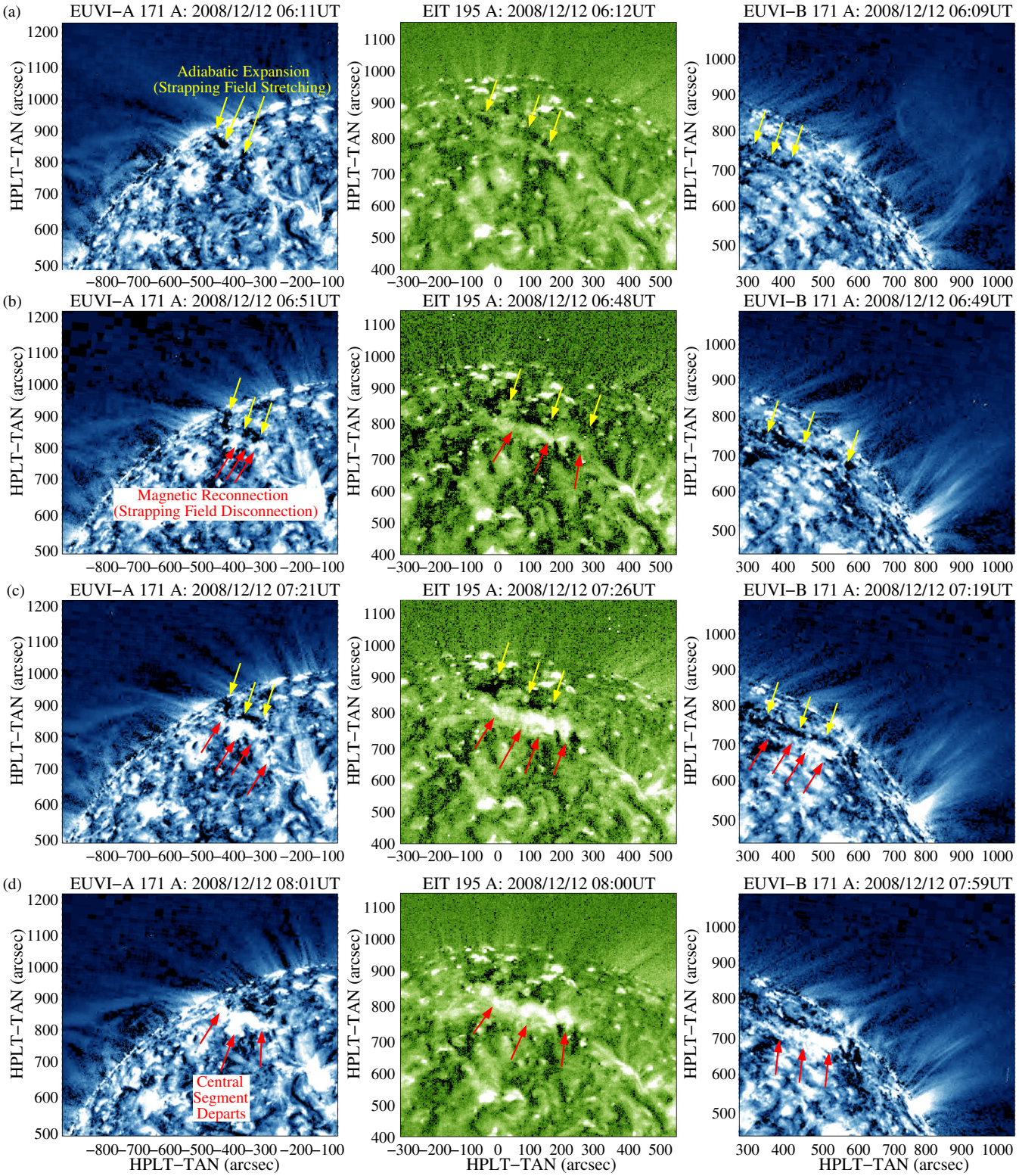

Figure 5. EUVI-A, EIT, and EUVI-B images indicating the passage of a dark front followed by a bright front moving toward the north as the western segment of the CME flux rope leaves the Sun. We attribute the former to the stretching of the surrounding strapping field by the erupting internal flux rope, followed by the surrounding field being wrapped underneath the central segment, and eventual disconnection via magnetic reconnection.

(An animation and a color version of this figure are available in the online journal.)

of transient flux rope behavior. We regard this as evidence of expansion of the containing magnetic flux bundle together with adiabatic expansion (darkening) of the confined material, followed by magnetic reconnection and associated heating and chromospheric evaporation (brightening). We postulate that the surrounding strapping field, which at the time of the departure of the central segment was still connected to the Sun, stretched and expanded adiabatically, which is manifested as the dark

front that is seen to expand to the east in EUVI-A. The legs of the strapping field were gradually brought together as the field lines were stretched, and they were finally disconnected from the Sun via magnetic reconnection. This is manifested as the bright front that begins in the west and expands eastward, engulfing the dark front.

Additionally, the bright front begins in a region surrounding the dark front, rather than upon the dark front itself. We regard this as evidence that the surrounding strapping field was dragged underneath the erupting central segment prior to reconnection. By 07:30 UT the transient fronts have disappeared, and this combination of initial core flux rope and a surrounding flux rope formed from the dragged and reconnected strapping field has also left the Sun. Note that the overall structure of the flux rope by this time is already distorted, with the western segment (described by DeForest et al. 2013) moving ahead of the central segment. The eastern segment remains stationary and visible for many hours after the liftoff of the central segment.

The two mechanisms that caused the eruption of the western and central segments describe two different physical scenarios, yet they are both involved with the launch of segments of the same flux rope. The reconnection (flare) that released the western segment was likely not directly connected to the actual western segment, as evidenced by the lack of local heating signatures in the flux rope structure itself, but rather a tether cutting the surrounding strapping field that was holding down the western segment prior to the flare. In this way, an additional flux rope layer was formed around the western segment immediately upon launch, likely forming the collective structure that expanded and was later observed as the northern component of the December 12 CME (and did not impact the Earth or any in situ spacecraft). On the other hand, the central segment is launched via mass draining, and so its surrounding strapping field remained anchored to the Sun during its initial eruption. It was stretched and dragged under tension underneath the erupting central segment for around two hours before it finally began to magnetically reconnect and dislodge itself from the Sun. The reconnection did not occur simultaneously everywhere beneath the central segment, but rather it was "unzipped" eastward, presumably because the western part of the central segment was farther away than its eastern part because the central segment was being led by the western segment.

There is insufficient evidence to determine which of these two launch mechanisms is more energetic: indeed, by the time the western and central segments reach the fields of view of the coronagraphs, they appear as a single distorted CME (with multiple loops), with its northern component ahead of the southern component (see Section 4). We do see evidence of flux rope distortion (reported by Howard & DeForest 2012), showing the northern component moving continually farther ahead of the southern component, but we cannot determine whether this was caused by the energetics of the initial launch or because the southern component propagated through a more dense region of the solar wind. The latter scenario was suggested by Howard & DeForest (2012).

3.4.1. Relationship to the "Coronal Sheath"

We note that although the western and central segments and their immediate strapping fields, which are both shown as the pink feature depicted in Figure 5 of DeForest et al. (2013), are separated from the Sun by around 08 UT, it is likely that further overlying fields still remain connected to the Sun farther away. They are denoted the "coronal sheath" by DeForest et al. (2013) and are colored green and orange in their Figure 5. We do not consider these fields in detail in the present study because there is little or no evidence of their influence on the launch and early evolution of the flux rope.

We considered the possibility that only the central segment of the flux rope is associated with the solar-connected strapping fields observed by *ACE* and *Wind*, which may be an indicator that only part of the overlying strapping field was dragged underneath the central segment and magnetically reconnected. In that case, there would be no evidence of field line connectivity to the Sun for the western segment, which has its strapping field disconnected via tether cutting, or the eastern segment, which may have pushed much of the strapping field aside during the kink instability launch process (see, e.g., Fan 2005; Rachmeler et al. 2009). Unfortunately, we have no in situ data to verify or reject this conjecture because the western segment did not impact an in situ spacecraft.

3.5. Evidence for Bisection

By 16 UT on December 12, we see no further evidence of magnetic activity in the EUV images related to the departed western and central segments of the flux rope. This is not surprising because by then they are around 20 $R_\odot$ away. Up until this time, the eastern segment remained unchanged, visible as a cavity (with an enclosed filament) suspended above the limb in EUVI-A. At around 16 UT we observe the first signs of its final disconnection, beginning with a single kink, with several more following until its final disconnection at around 22 UT. This is shown in Figure 6. The persistence of the eastern segment at the Sun presents something of a puzzle because we see no evidence of field line stretching in any of the three data sets after the departure of the central segment at around 08 UT. One possible explanation is that the eastern segment was not part of the original magnetic structure that comprised the western and central segments, but this explanation also has difficulties and is described more fully in Section 5.1. Alternatively, the eastern segment, which was originally part of the prelaunch flux rope configuration, was separated from the rest of the flux rope some time after the removal of the central segment from the Sun. The cross-sectional scan described in Section 3.2 showed no signs of discontinuity throughout the five days prior to launch, which we take to be evidence of this latter scenario. In this case, the separation would likely have occurred via magnetic reconnection, and we have sought evidence of a retracting feature around the time and location of the eastern end of the eastern segment because such features are rarely observed and may be evidence of magnetic reconnection overhead.

Figure 7 shows a downward-moving (i.e., toward the Sun) jet in EUVI-B from 08:06 to 08:26 UT. We found a faint feature in EUVI-A (not shown). We did not see the feature with EIT, which may be due to its coarser spatial resolution and higher background level than EUVI. We submit this as possible evidence for the bisection of the flux rope at around 08 UT. If the signature in Figure 7 was, in fact, a retracting feature from the bisection of the flux rope via magnetic reconnection, then the reconnection occurred very quickly (within 30 minutes) after the separation of the last of the strapping field accompanying the central segment from the corona. The result would be no stretching of the separated connected eastern segment, which from the moment of bisection can be regarded as a separate flux rope.

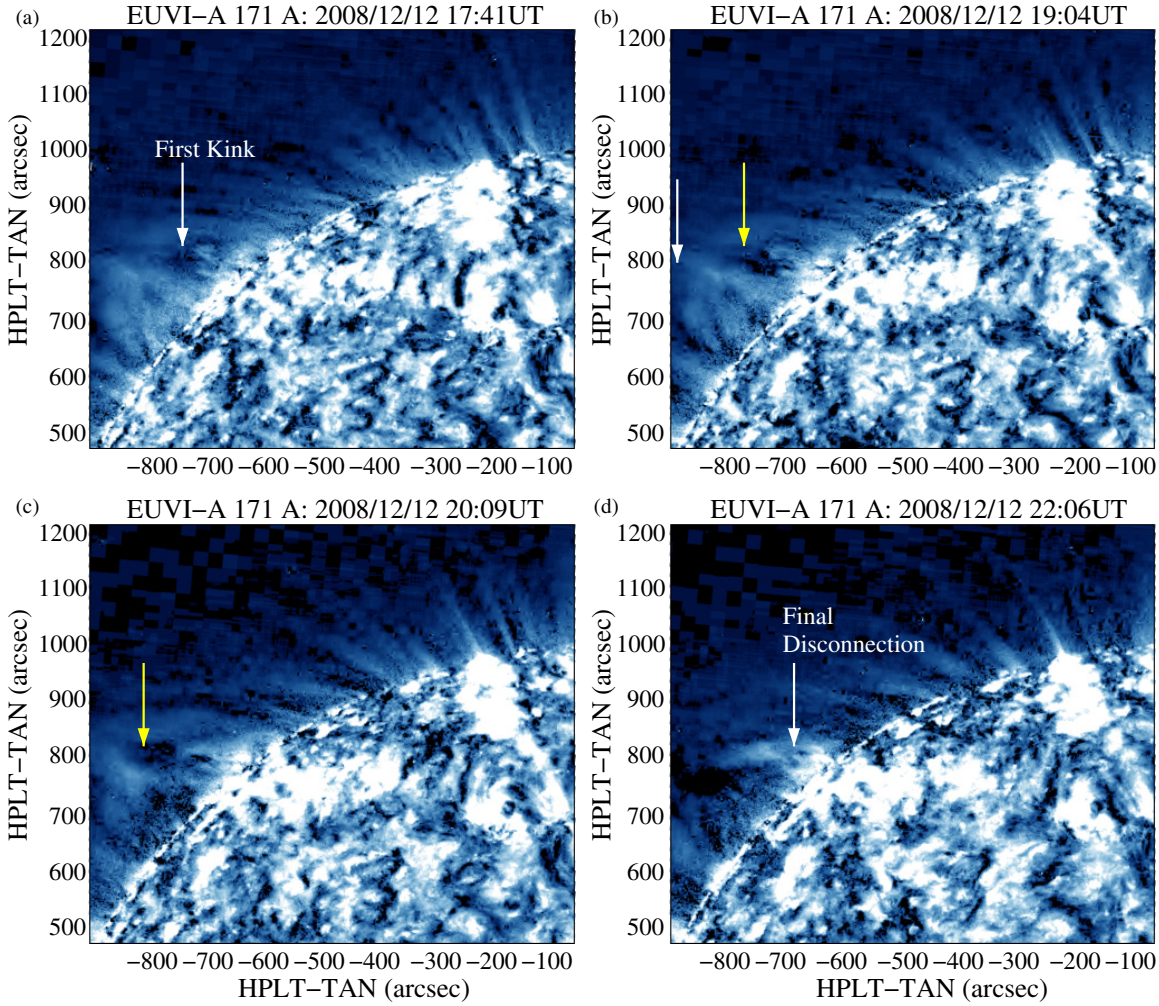

Figure 6. Sequence of EUVI-A images showing the launch of the easternmost segment of the flux rope. This is launched via the kink instability mechanism, with (a) the first kink appearing at 17:41 UT, (b) several kinks following (image shown at 19:04 UT; (c) shown at 20:09 UT), and (d) its final disconnection from the Sun at 22:06 UT.

(An animation and a color version of this figure are available in the online journal.)

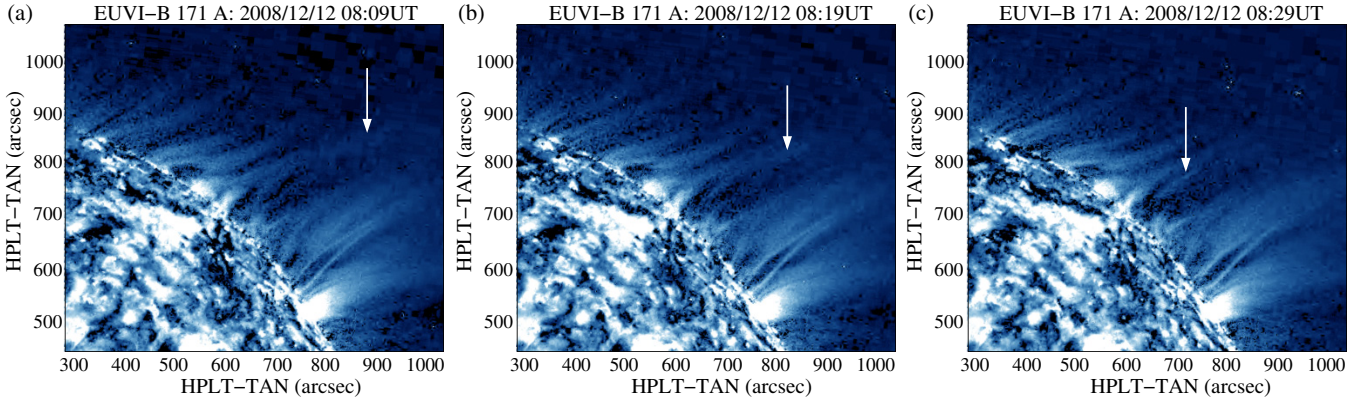

Figure 7. (a–c) Sequence of EUVI-B images with the passage of a retracting jet indicated by the white arrows. This may be evidence of the bisection of the CME flux rope at around 08 UT.

(An animation and a color version of this figure are available in the online journal.)

4. FARTHER FROM THE SUN

Consider the coronagraph and heliospheric images in Figure 8. Panel (a) shows COR2 images (from *STEREO-A* on the left, *STEREO-B* on the right) of the 2008 December 12 CME that has been reported by many workers (Section 2). We highlight three distinct regions within the CME envelope in COR2-A and two in COR2-B. Traditionally, such structures might be

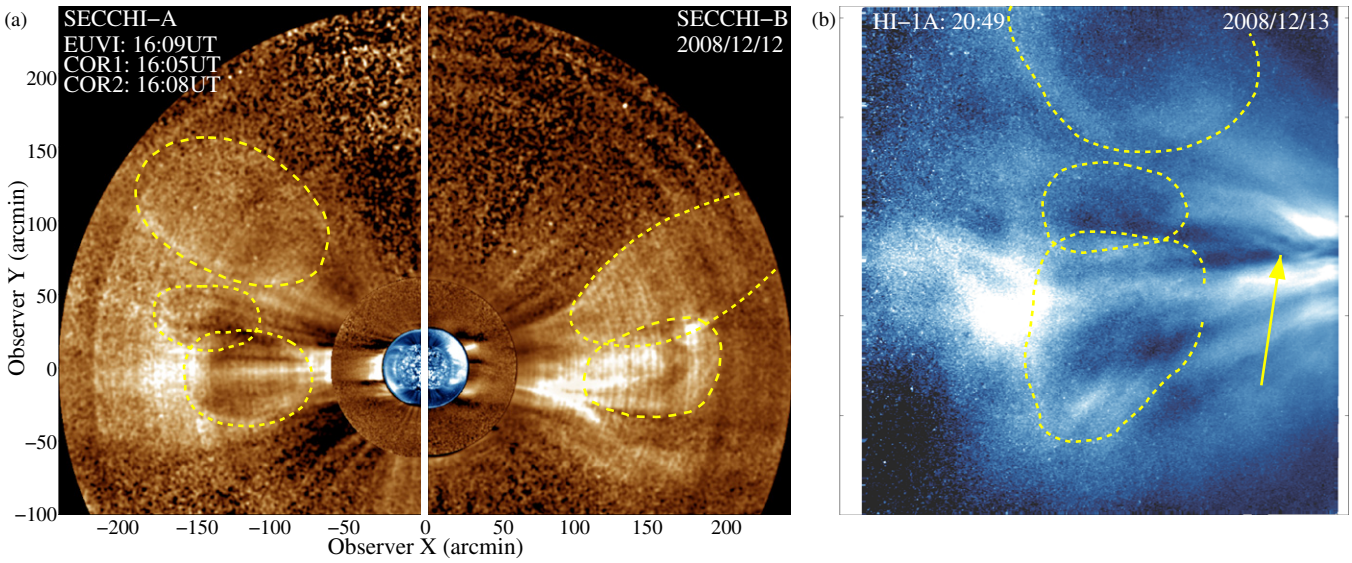

Figure 8. White-light images of the CME flux rope. (a) *STEREO-A* (left) and *STEREO-B* (right) COR2 image at 16:20 UT on 2008 December 12, with embedded accompanying COR1 and EUVI images. Dashed regions indicate the cavities in the COR2 images, which appear to be separate CME structures. These are actually manifestations of the same flux rope (segments 1 and 2 from DeForest et al. 2013), seen at an angle. (b) HI-1A image from 20:49 UT on 2008 December 13, with four features indicated. The first three are the same as those in Panel (a), and the fourth (arrowed) is the signature of the final (easternmost) segment of the flux rope. These typically would be regarded as four separate eruptive phenomena, but, according to our primary narrative, they are all manifestations of the same prelaunch flux rope. (A color version of this figure is available in the online journal.)

labeled as multiple CMEs (e.g., Bemporad et al. 2012; Liu et al. 2012) or perhaps multiple loops within a single CME (e.g., Patsourakos et al. 2013), but they are, in this case, manifestations of the same CME flux rope (the western and central segments), seen at different depths and at an angle to the observer. Likewise, Panel (b) shows a Heliospheric (HI-1A) image of the same CME followed by an apparent U-shaped structure. The latter is the signature of the eastern segment leaving the corona, which disconnected from the Sun at 22 UT on December 12. Inspection of the SECCHI movies provided by Howard & DeForest (2012) and Howard et al. (2012) demonstrate the continuity of the evolution of this final feature. It is denoted "P1" by Howard et al. (2012) and cited as a possible source of density increases within the in situ MC. We now recognize this feature as the final disconnection of the eastern segment spanning considerably to the east of the Earth-impacting central segment.

4.1. Magnetic Cloud at STEREO-B: Further Evidence of the Kink Instability?

Howard & DeForest (2012, their Figure 2) show the signatures of a weak MC at *STEREO-B* starting around 08 UT on December 16. There they saw it as evidence of the same flux rope that impacted the Earth a day later. The *STEREO-B* MC had around twice the diameter of the one observed by *ACE* and *Wind*, and, as noted by Howard et al. (2012, their Section 6.1), had a field rotation in the opposite direction of that observed at the Earth. More precisely, the field observed by *ACE* had a central axis of $(x, y, z)_{\rm RTN} \sim (-1, -1, 0)$, and that observed at *STEREO-B* was $(x, y, z)_{\rm RTN} \sim (-1, 1, -1)$. This orientation is consistent with the *ACE*/*Wind* MC being formed by an unrotated flux rope (the central segment) and the *STEREO-B* MC being formed separately by the writhed eastern segment of the preeruption structure due to the kinking/writhing mechanism of its liftoff.

We attribute the fast arrival of the eastern segment at *STEREO-B* (the average travel time of the eastern segment to 1 AU was 85 hr, compared with 120 hr for the central segment) to three possibilities: (1) the rapid rate of expansion immediately after launch, which was observed to be twice the rate of the western and central segments as observed by EUVI and indicative of a more energetic launch; (2) its passage through a less-dense region of the solar wind—compare the densities of the ambient solar wind measured by *Wind* (10 $\rm cm^{-3}$; DeForest et al. 2013) with those of *STEREO-B* (5 $\rm cm^{-3}$; Howard & DeForest 2012); or (3) a combination of (1) and (2). The solar wind speed is identical in *STEREO-B* and *Wind* ($\sim$340 km $\rm s^{-1}$), so this is not a discriminating factor. The absence of a density buildup ahead of the MC in *STEREO-B* (Howard & DeForest 2012, their Figure 2), compared with a gradual twofold increase of the density observed by *Wind*, may be indicative of a less dense solar wind stream at *STEREO-B*, or it may be a signature of a reduction or absence of a strapping field surrounding the eastern segment (see Section 3.4.1). In the absence of observations at all stages of the evolution of the eastern segment, we can only speculate as to the nature of the strapping field surrounding it.

5. DISCUSSION

When we first selected this CME for analysis (DeForest et al. 2011), we did so because we thought that the 2008 December 12 CME was as simple a CME as could be expected: a slow, symmetric, classic, three-part CME erupting during the quietest period of solar activity in the modern era. Through multiple studies, we have found this event to be far from simple. For this single event, we have identified evidence of

1. a flux rope that was preformed, being established five days prior to launch;
2. an extended flux rope structure erupting asymmetrically from one end to the other;
3. three separate onset mechanisms required to completely dislodge the flux rope from the solar corona;
4. expansion and disconnection of parts of the surrounding strapping field;

5. bisection of the original flux rope;
6. multiple and spatially separated white-light signatures of the same initial flux rope;
7. the surrounding "coronal" field being stretched by the flux rope as far out as 1 AU; and
8. kinking of a flux rope segment, leading to a rotation before and during launch, with the resulting changes in orientation near 1 AU.

Figure 9 shows an idealized cartoon of the evolution of this flux rope. We have accounted for the magnetic field regimes inferred to be at play during its launch, and included the time and likely location of the bisection. This figure describes the narrative derived from the multiple papers we have published on this event and the observations presented in the present paper. It also demonstrates the level of complexity of the physical mechanisms required to completely remove this flux rope from the Sun and the importance of taking projection into consideration when interpreting different data sets. The latter has important implications for developing areas in solar physics, including those involving multiple and interacting CMEs. We have shown that apparent multiple structures can in fact be projected manifestations of the same complete initial structure.

By way of summary, we describe, with direct reference to the cartoon in Figure 9, our flux rope narrative of the launch of this greater CME structure from the Sun.

(a) shows the prelaunch magnetic configuration of the three segments of the flux rope (red, magenta, green), the overlying strapping field (black), the anchor field (orange), and the filament (yellow at the base of the loops). The anchor field is held to the Sun by filament material at the base of its single loop, and it wraps over the top of the central (magenta) segment, preventing it from launching (see DeForest et al. 2013).

(b) shows the initial flare (red), first seen at 03:12 UT and moving westward such that by 03:36 UT it spanned the region beneath the western segment (Figure 2(b)). The flare is a manifestation of the initial launch of the flux rope, occurring via the disconnection of the strapping field via magnetic reconnection, removing first the eastern part (the second-to-last black loop) and then the western part (the last black loop) of the western segment. The black loops now form a complete spiral, resembling the inner western segment, which collectively begin to move away from the Sun. The filament material at the base moves with the loops, and the material at the base of the orange loop (the anchor) begins to move along the orange loop westward.

(c) shows the launch of the central segment, brought about by the draining of the anchoring filament material from the anchor field (orange loop) into the Sun to the southwest of the original flare location (Figure 4). The western segment and its surrounding (now disconnected) strapping field continue to move away from the Sun and have expanded, dragging the central segment, now free to depart because of the removed anchoring filament, with it. Unlike the western segment, however, the strapping field surrounding the central segment remains attached to the Sun and is stretched (i.e., adiabatically expanded) by the erupting central segment, and their footpoints are dragged toward each other. The stretching is manifested as a darkening in the EUV images (Figure 5). The filament material at the base of the central segment is carried with the erupting flux rope.

(d) shows the magnetic reconnection and disconnection of the strapping field surrounding the central segment, beginning around two hours after the central segment departed, and it is now some considerable distance from the Sun (Figure 5). The reconnection begins from the western part of the field and is "unzipped" eastward. This finally completes the outer layer of the central segment of the flux rope, which joins the western segment to form the cavity of the December 12 CME. The coronagraphs and Heliospheric Imagers (HIs) on *STEREO-A* observed the flux rope from an angle, with the western segment ahead of and farther away from the plane of the sky than the central segment. This created the illusion of multiple loops within a CME, when they were in fact two optically thin cross sections of the same flux rope. It is unclear whether the outer edges of the central cavity are the two segments or their disconnected strapping fields. The solution will determine the rate of expansion of the original flux rope (the two segments).

(e) shows the bisection event at around 08 UT (first observed as a retracting feature in EUVI-B at 08:06 UT: Figure 7). Given the distance between the central and eastern segments at this time, we speculate that there are several points of magnetic reconnection along the sheet between the two segments and their surrounding flux ropes. There is no evidence of a response from the eastern segment, which remains fixed to the Sun.

(f) shows the first twist in the eastern segment at 16 UT (Figure 6). The twist is from south to north. At this time the western and central segments are around 12 $R_\odot$ away.

(g) shows the final liftoff of the eastern segment at 22 UT (Figure 6). The western and central segments are now around 35 $R_\odot$ away. The final segment is manifested as a U-shaped eruption in the coronagraph and HI images. This is most likely the filament material, seen suspended within the loop in EUVI-A throughout its lifetime and lifting off with it. We can only speculate as to the nature of the strapping field during the launch and evolution of the eastern segment. We depict it in Figure 9 as being pushed aside during launch, but it is also possible that it may be dragged into the heliosphere, at least for a while.

Its strapping field is mostly pushed aside during launch, such that only the eastern segment and a small part of its surrounding field are carried into the solar wind.

(h) shows the configuration of the complete flux rope at 00 UT on December 17, when *ACE*/*Wind* was in the "coronal sheath" of the central segment and *STEREO-B* was just emerging from the other side of the eastern segment. We show the closed MC comprising the central segment and its closed strapping field combined. We extend the strapping field to the western segment, and although we have no information about its structure here (because the western segment did not impact an in situ spacecraft; see Section 3.4.1), we show it as a continuous extension of the central segment. The eastern segment, now completely separated from the central segment, has little or no associated strapping field, and we represent the twisting from the kink instability as a series of overlapping loops. It is ahead of the western and central segments, despite it being launched around 18 hr after them. This is attributed to either a higher energetic state of the launching mechanism or (more likely) to the passage through a region of a stream of lower solar wind density.

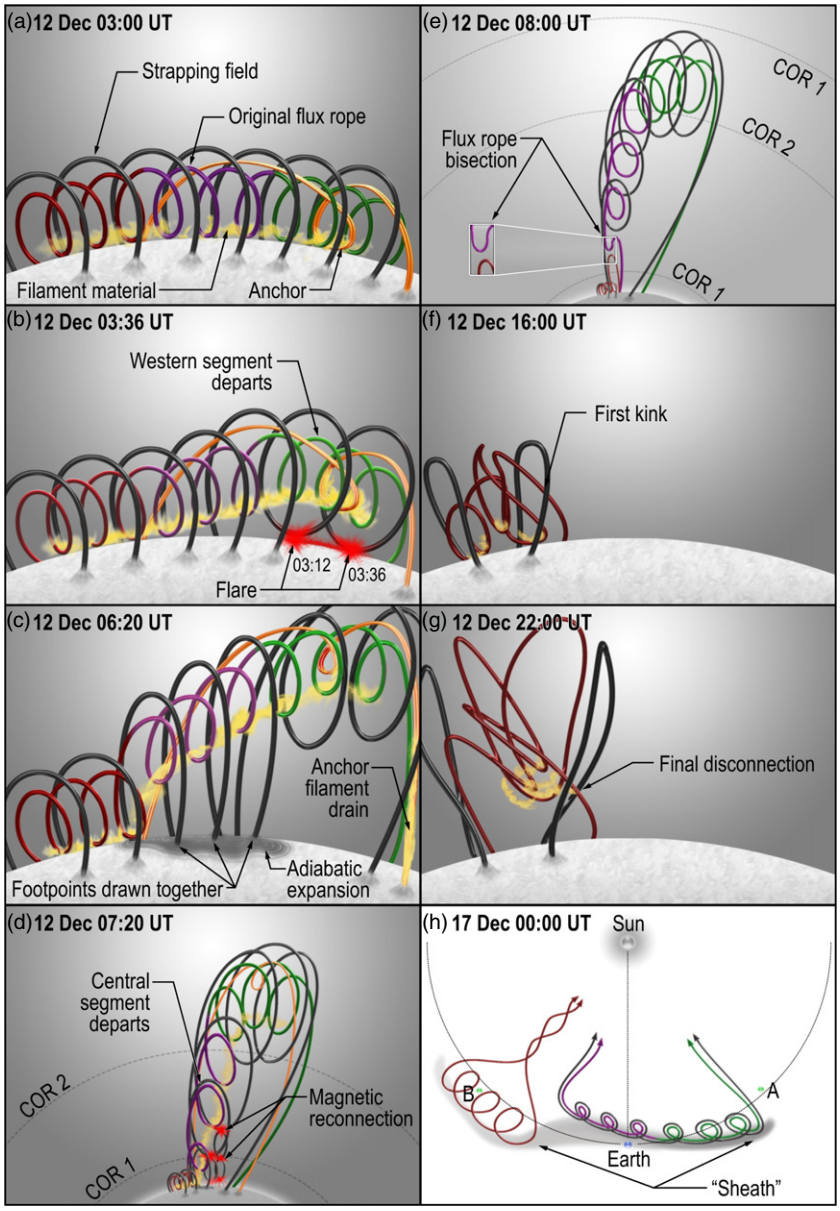

Figure 9. Idealized cartoon of our narrative describing the launch of the 2008 December CME flux rope. Note that the flux rope here is straight, but its actual alignment on the Sun is highly curved (see Figure 1). Each panel is described in detail in the accompanying text and only briefly summarized here. (a) The prelaunch configuration of the magnetic flux rope, with the three segments, strapping field, anchor field, and filament. (b) The initial launch of the western segment is manifested as a solar flare, which indicates the tether-cutting of the surrounding strapping field. (c) The launch of the central segment by the removal of the tension from the anchor field, which has been drained of its filament material. (d) Eventual disconnection of the strapping field surrounding the central segment, via magnetic reconnection brought about by its stretching and dragging underneath the central segment. (e) The magnetic reconnection event that bisects the field between the central and eastern segments. (f) The first twist of the kink instability that initiates the launch of the eastern segment. (g) The launch of the eastern segment via the kink-instability mechanism. (h) The configuration of the three segments at 00 UT on December 17, when the central segment passed through *ACE*/*Wind* and the eastern segment passed through *STEREO-B*. A time stamp is provided for each panel, and features of interest are indicated with the labels.

(A color version of this figure is available in the online journal.)

5.1. Alternative Narratives

Although the launch and evolution we have depicted in Figure 9 is our view of the most likely scenario surrounding the magnetic structure giving rise to the 2008 December 12 CME, other narratives have been constructed that describe the observations. These narratives, developed by other authors, rely on implausible coincidences or are falsified by a more complete analysis of the available data. In the interest of completeness, we present two such alternative narratives in the following sections.

Figure 10 shows a PFSS (e.g., Wang & Sheeley 1992) rendering of the prelaunch magnetic configuration of 2008 December 12 (O. Panasenco 2014, private communication; see also Panasenco et al. 2011, 2013). Panel (d) shows the centralized view at higher resolution, with two separated filament channels aligned along the same neutral line. This model presents the possibility that there are two separate magnetic structures prior to launch. The implication here is that the eastern segment (the red component in Figures 1(a) and 9) was always separate from the central and western segments, and it is shown in Figure 10 as the structure running almost perpendicularly southward away from the main magnetic structure. The physical argument in favor of this (O. Panasenco 2014, private communication) is that such a highly bent magnetic configuration is too energetically

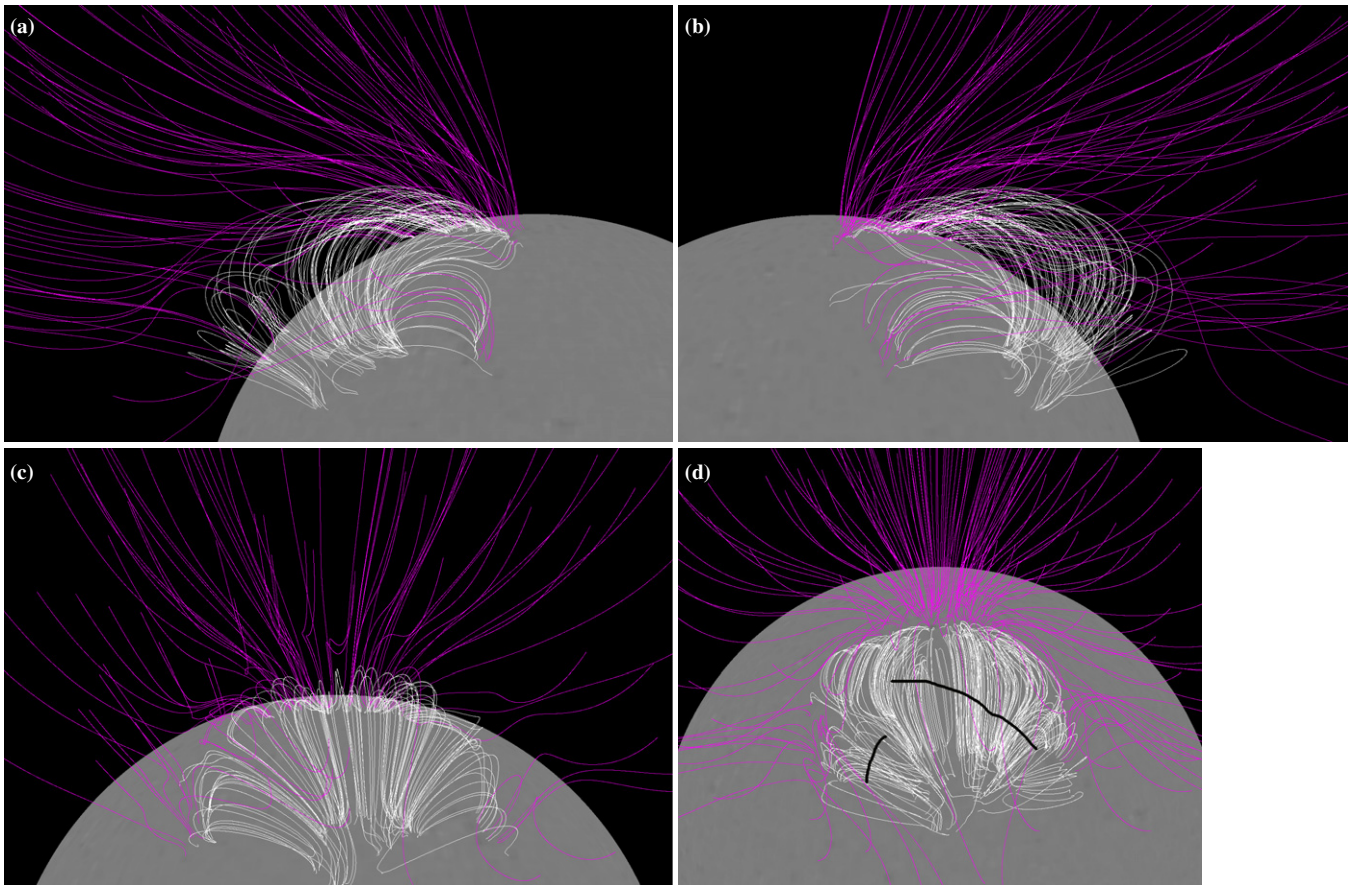

Figure 10. Potential field source surface (PFSS) rendering of the prelaunch magnetic configuration on 2008 December 12 (O. Panasenco 2014, private communication). We present this rendering as it would be observed from (a) *STEREO-A*, (b) *STEREO-B*, and (c) *SOHO*. Image (d) shows a higher resolution PFSS rendering of the same structure, observed directly from above. The dark curves indicate the suggested location of two separate filament channels, possibly aligned along the same neutral line. See also Panasenco et al. (2011, 2013) for further examples of the PFSS rendering for this CME.

(A color version of this figure is available in the online journal.)

unstable to be a continuous structure. Such a scenario does not require a bisection event to explain the different behaviors of the western and central versus the eastern segments, nor does it necessarily require the kinking of a magnetic field to describe the different chirality of the MC observed at *ACE* and *Wind* versus the one observed by *STEREO-B*. Also, observationally, the PFSS rendering agrees fairly well with the loops observed over the limb in *STEREO-A* and *STEREO-B* (Figures 10(a) and (b), respectively) and with the brightening of the arcade observed by EIT (Figures 10(c)). All of the other physical explanations, including onset mechanisms and the strapping field stretching and reconnecting, apply equally well to this alternative narrative.

If the multiple-structure scenario held, we would expect to see evidence of a discontinuity in our cross-sectional scan (described in Section 3.2) throughout the days leading up to the launch. We found no such evidence of a separation in the continuity of the magnetic structure. We do note, however, that the PFSS rendering shows a field with a large cross section that may not be easily traceable and that we do observe a reduction in height of the suspended filament throughout the scan. Second, this scenario does not account for the observation of the rarely observed retracting feature after the complete departure of the central segment. Finally, we note that the PFSS rendering places the separate structure considerably to the west of *STEREO-B* (the central meridian of Figure 10(b)), and therefore it cannot account for the MC signatures that we observed there. While these pieces of seemingly contradictory evidence are by no means conclusive, they collectively lead us to a tendency to favor the complete flux rope narrative presented in Section 5 and depicted in Figure 9.

Figure 10 also presents a diagram of a second alternative narrative. Here we consider that the prelaunch CME was not a flux rope at all, but rather the flux rope was formed only after the field had departed from the Sun.[1] One narrative, reported by, e.g., Panasenco et al. (2011, 2013, 2014), describes the prelaunch configuration in terms of a filament channel topological system comprising a filament spine, an overlying sheared (writhed) field strapped with coronal loops (see, e.g., Panasenco et al. 2014, their Figure 2). A detailed discussion of the 2008 December CME in the context of this alternative narrative is presented by Panasenco et al. (2011). Their evidence includes the difference in propagation direction between the filament eruption and the accompanying CME.

Although the prelaunch nonflux rope narrative is not physically implausible, we once again have a tendency to favor the flux rope narrative presented throughout this paper. Although there is certainly no conclusive evidence for either narrative for this event, one unresolved issue regarding the nonflux rope

[1] The authors note that Figure 10 is necessarily biased toward presenting a nonflux rope alternative narrative because PFSS is incapable of producing a flux rope configuration.

narrative involves the presence of the cavity in the prelaunch configuration. The sheared field overlying the filament is described as the "cavity field" by Panasenco et al. (2014), but we have not yet encountered a physical description, to our satisfaction, of why this cavity field should be absent of material while the surrounding filament and coronal fields are not. We anticipate that such a description may be explored in future discussions and papers regarding the prelaunch magnetic configuration of a CME flux rope.

6. CONCLUDING REMARKS

This paper is the final one in a series of five that we have published on the December 12 CME and its flux rope. We have found a surprising level of complexity in the structure and eruption of the flux rope, and its implications for CME observation in both EUV and white light are clear. While we can describe the launch of the flux rope in terms of existing CME onset models, we require three separate models to completely dislodge it from the Sun. We offer this narrative as evidence that not only are multiple-onset mechanisms possible for CMEs, but that multiple mechanisms may be required to dislodge even a single magnetic structure from the Sun.

To conclude, we offer our contribution to a question raised in a dedicated session at the 2013 SHINE Workshop: "What is a CME?" Given the most recent observations from *STEREO* and *SDO*, it seems that a working ubiquitous definition of a CME is as difficult to describe as it has ever been. While we prefer a physical, rather than observational, definition of the term, it seems that the only meaningful physical definition would be to identify a signature of a driver within the CME, and we now recognize the flux rope (FR) as the main provider to the driving force of at least the classic three-part CME (Vourlidas et al. 2013, for example, have suggested the term "FR-CME" as a separate category). This poses an observational constraint, however, because a single flux rope can actually be manifested as several CMEs in a coronagraph or heliospheric imager, as our results have shown. Is it meaningful, then, to regard them as separate phenomena if they all have the same driving mechanism? How can we distinguish between those that have a common driver and those that do not? We were able to take advantage of the quadrature of the *STEREO* spacecraft for our study of this event, which, along with the centrally located Earth as an additional observer, is unique in the *STEREO* era.

Finally, the importance of 3D perspective regarding CME and flux rope observations cannot be overstated. In the case presented here (Section 4), we have several separate structures in coronagraph and heliospheric images, one of which is separated by around 20 $R_\odot$ from the others when they were all within 0.5 AU, yet our narrative describes their origin at the Sun as the same flux rope. The flux rope spans a longitudinal range of some 90°, meaning that the white-light imagers only observe a cross section of the entire flux rope, which, when observed at an angle (such as from *STEREO-A* for our case), can appear as two separate CME cavities. They are not interacting or overlapping CMEs, but rather are part of a continuous structure extending toward and away from the observer, probably for many 10s of degrees. Observations are further complicated by the fact that different segments of the flux rope can be launched by different onset mechanisms, further impeding our ability to confidently identify isolated events.

The authors gratefully thank O. Panasenco for invaluable discussions regarding the alternative narratives and for her provision of the PFSS renderings used in Figure 10. We also thank S. Gibson for helpful discussions throughout the development of this paper, and Richard Menchaca of the Space Science and Engineering Art Department (SwRI) for his production of Figures 1 and 9. The *STEREO*/SECCHI pipeline was developed with support from NASA Grant NNG05GK14G. We thank NASA, NRL, and RAL for their maintenance and provision of the SECCHI data set. This work is supported under the NASA H-GI program (Grant NNX13AE01G) and the NSF SHINE Competition (grant AGS-1260321).

REFERENCES

Antiochos, S. K., DeVore, C. R., & Klimchuk, J. A. 1999, ApJ, 510, 485
Bemporad, A., Zuccarello, F. P., Jacobs, C., Mierla, M., & Poedts, S. 2012, SoPh, 281, 223
Bothmer, V., & Schwenn, R. 1998, AnG, 16, 1
Burkepile, J. T., Hundhausen, A. J., Stanger, A. L., St. Cyr, O. C., & Seiden, J. A. 2004, JGR, 109, A03103
Burlaga, L., Sittler, E., Mariani, F., & Schwenn, R. 1981, JGR, 86, 6673
Byrne, J. P., Maloney, S. A., McAteer, R. T. J., Refojo, J. M., & Gallagher, P. T. 2010, NatCo, 1, 74
Cane, H. V., & Richardson, I. G. 2003, JGR, 108, 1156
Cane, H. V., Richardson, I. G., & Wibberenz, G. 1997, JGR, 102, 7075
Chen, J. 1989, ApJ, 338, 453
Davis, C. J., Davies, J. A., Lockwood, M., et al. 2009, GeoRL, 36, L08102
DeForest, C. E., Howard, T. A., & McComas, D. J. 2013, ApJ, 769, 43
DeForest, C. E., Howard, T. A., & Tappin, S. J. 2011, ApJ, 666, 576
Delaboudinière, J.-P., Artzner, G. E., Brunaud, J., et al. 1995, SoPh, 162, 291
Eyles, C. J., Harrison, R. A., Davis, C. J., et al. 2009, SoPh, 254, 387
Eyles, C. J., Simnett, G. M., Cooke, M. P., et al. 2003, SoPh, 217, 319
Fan, Y. 2005, ApJ, 630, 543
Fan, Y., & Gibson, S. E. 2003, ApJL, 589, L105
Fan, Y., & Gibson, S. E. 2004, ApJ, 609, 1123
Fong, B., Low, B. C., & Fan, Y. 2002, ApJ, 571, 987
Forbes, T. G., Linker, J. A., Chen, J., et al. 2006, SSRv, 123, 251
Gibson, S. E. 2005, AGUSM, SP43C-01
Goldstein, H. 1983, in JPL Solar Wind Five, ed. M. Neugebauer (Hampton, VA: NASA STI), 731
Gosling, J. T. 1990, GMS, 58, 9
Hood, A. W., & Priest, E. R. 1981, GApFD, 17, 297
Howard, R. A., Moses, J. D., Vourlidas, A., et al. 2008a, SSRv, 136, 67
Howard, T. A., & DeForest, C. E. 2012, ApJ, 746, 64
Howard, T. A., DeForest, C. E., & Reinard, A. A. 2012, ApJ, 754, 102
Howard, T. A., Nandy, D., & Koepke, A. C. 2008b, JGR, 113, A01104
Illing, R. M. E., & Hundhausen, A. J. 1985, JGR, 90, 275
Klein, L. W., & Burlaga, L. F. 1982, JGR, 87, 613
Klimchuk, J. A., & Sturrock, P. A. 1992, ApJ, 385, 344
Lepping, R. P., & Berdichevsky, D. 2000, Recent Res. Devel. Geophys., 3, 77
Lepping, R. P., Jones, J. A., & Burlaga, L. F. 1990, JGR, 95, 11957
Liu, Y., Davies, J. A., Luhmann, J. G., et al. 2010, ApJL, 710, L82
Liu, Y. D., Luhmann, J. G., Möstl, C., et al. 2012, ApJL, 746, L15
López Ariste, A., Aulanier, G., Schmeider, B., & Saubz Dalda, A. 2006, A&A, 456, 725
Low, B. C. 1993, BAPS, 25, 1218
Lugaz, N. 2010, SoPh, 267, 411
Lynch, B. J., Antiochos, S. K., DeVore, C. R., Luhmann, J. G., & Zurbuchen, T. H. 2008, ApJ, 683, 1192
Lynch, B. J., Zurbuchen, T. H., Fisk, L. A., & Antiochos, S. K. 2003, JGR, 108, 1239
Martin, S. F., Livi, S. H. B., & Wang, J. 1985, AuJPh, 38, 929
Marubashi, K. 1986, AdSpR, 6, 335
Moore, R. L., & Sterling, A. C. 2006, GMS, 165, 43
Panasenco, O., Martin, S. F., Joshi, A. D., & Srivastava, N. 2011, JASTP, 73, 1129
Panasenco, O., Martin, S. F., & Velli, M. 2014, SoPh, 289, 603
Panasenco, O., Martin, S. F., Velli, M., & Vourlidas, A. 2013, SoPh, 287, 391
Patsourakos, S., Vourlidas, A., & Stenborg, G. 2010, ApJL, 724, L188
Patsourakos, S., Vourlidas, A., & Stenborg, G. 2013, ApJ, 764, 125
Rachmeler, L. A., DeForest, C. E., & Kankelborg, C. C. 2009, ApJ, 693, 1431
Sturrock, P. A. 1989, SoPh, 121, 387

Temmer, M., Veronig, A. M., Kontar, E. P., Krucker, S., & Vršnak, B. 2010, ApJ, 712, 1410
Tian, H., Tomczyk, S., McIntosh, S. W., et al. 2013, SoPh, 288, 637
Titov, V. S., & Démoulin, P. 1999, A&A, 351, 707
Török, T., & Kleim, B. 2003, A&A, 406, 1043
Török, T., & Kleim, B. 2005, ApJL, 630, L97
van Ballegooijen, A. A., & Martens, P. C. H. 1989, ApJ, 343, 971
Vourlidas, A., Lynch, B. J., Howard, R. A., & Li, Y. 2013, SoPh, 284, 179
Wang, Y. M., & Sheeley, N. R., Jr. 1992, ApJ, 392, 310
Webb, D. F., Cliver, E. W., Gopalswamy, N., Hudson, H. S., & St. Cyr, O. C. 1998, GeoRL, 25, 2469
Wood, B. E., Karovska, M., Chen, J., et al. 1999, ApJ, 512, 484
Zhang, M., & Low, B. C. 2004, ApJ, 600, 1043